The Astrophysical Journal, 573:778–788, 2002 July 10
© 2002. The American Astronomical Society. All rights reserved. Printed in U.S.A.

HIDING IN PLAIN SIGHT: *CHANDRA* OBSERVATIONS OF THE QUIESCENT NEUTRON STAR 4U 2129+47 IN ECLIPSE

Michael A. Nowak
Massachusetts Institute of Technology, Center for Space Research, 77 Massachusetts Avenue, Cambridge, MA 02139; mnowak@alum.mit.edu

Sebastian Heinz
Max-Planck-Institut für Atrophysik, Karl-Schwarzschild-Strasse 1, 85740 Garching, Germany; heinz@mpa-garching.mpg.de

and

M. C. Begelman
JILA and Department of Astrophysical and Planetary Sciences, University of Colorado at Boulder, Campus Box 390, Boulder, CO 80309; mitch@jila.colorado.edu
Received 2001 November 29; accepted 2002 March 19

ABSTRACT

During a previous outburst phase, the neutron star 4U 2129+47 exhibited evidence for a spatially extended accretion disk corona via broad, partial X-ray eclipses occurring periodically on the 5.24 hr orbit. Since 1983, however, 4U 2129+47 has entered a quiescent state several orders of magnitude fainter. We have performed a 37 ks (≈two binary orbits) *Chandra* observation of 4U 2129+47 to determine whether an extended coronal structure also exists in quiescence. Total eclipses are found, and the rapidity of the eclipse ingress and egress is used to place upper limits on the size of the X-ray source. The spectrum is found to be comprised of a soft component plus a fairly hard power-law tail. The former is seen to be sinusoidally modulated over the orbital period in a manner consistent with neutral column variations, possibly due to the interaction of an accretion stream with a (small) disk about the neutron star. We fit realistic neutron star atmosphere models to the soft spectra and comment on the consistency of the spectra with cooling neutron star models. It has been previously suggested that the 4U 2129+47 system is a hierarchical triple, with the outer body being an F star. We use differential astrometry to show that the X-ray point source and F star are spatially coincident to within 0″.1. We further compare newly determined upper limits for the extrinsic neutral column to the reddening of the F star. Finally, we discuss how future X-ray observations can further constrain models of quiescent neutron star emission as well as directly verify the triple hypothesis.

Subject headings: accretion, accretion disks — stars: individual (4U 2129+47) — stars: neutron — X-rays: stars

1. INTRODUCTION

Accretion disk corona (ADC) sources such as 4U 2129+47 are believed to be near edge-on accreting systems since they have shown binary orbital modulation via broad, partial X-ray eclipses. Such eclipses imply emission extended over radii comparable to the binary separation (McClintock et al. 1982; White & Holt 1982). Studies of the ADC X1822−371 offer an intriguing possibility for the cause of this very extended corona (Heinz & Nowak 2001). Orbital period derivative measurements imply that X1822−371 may be accreting very close to its Eddington rate; however, only a very small fraction of the Eddington flux is observed. If the mass transfer from the secondary is actually accreted by the primary, then the ADC must be either very optically thin (the tacit assumption made for "on-state" emission of 4U 2129+47 by Garcia & Grindlay 1987) or very optically thick. If the latter is true, the released accretion energy may not be able to diffuse out of the flow on a viscous inflow timescale, and the corona will essentially become an advection-dominated accretion flow (Esin, McClintock, & Narayan 1997 and references therein). In order to dissipate the accretion energy, an adiabatic outflow might ensue at a large radius (adiabatic inflow/outflow solution [ADIOS]; Blandford & Begelman 1999), hence creating the ADC.

The ADC source 4U 2129+47 is strongly believed to be a neutron star since it has exhibited a type I X-ray burst (Garcia & Grindlay 1987). Its classification as an ADC is due to the fact that prior to 1983, 4U 2129+47 was observed to have a light curve similar to that of X1822−371. Over the 5.24 hr orbit of 4U 2129+47, the eclipse width was ≈0.2 in phase and ≈75% of the X-rays were occulted at the eclipse midpoint. As hypothesized for X1822−371, the ADC might have been indicating the presence of an ADIOS.

Since 1983, 4U 2129+47 has been in a quiescent state. The question then arises as to whether the extended coronal structure has persisted or recurred in this state (see Garcia 1994; Garcia & Callanan 1999). An extended coronal structure could signal the presence of an ADIOS, albeit at low accretion rates where advection domination might ensue because of a decoupling of the ions and electrons. The bulk of the accretion energy would be stored as thermal energy of the protons, which would then be lost as a wind rather than dissipated on the neutron star surface (Blandford & Begelman 1999).

Alternatively, the spectra of quiescent neutron star sources might be due to emission from their surface as they cool after a prior active accretion phase to a low level of residual accretion (van Paradijs et al. 1987; Brown, Bildsten, & Rutledge 1998; Rutledge et al. 2000; Bildsten & Rutledge 2001). Thermal emission from the neutron star surface has been

suggested as partly contributing to the putative differences between the fluxes of quiescent neutron stars and quiescent black hole candidates, with the former class being suggested as systematically brighter (Narayan, Barret, & McClintock 1997a; Bildsten & Rutledge 2001; Garcia et al. 2001). Modern neutron star atmosphere models utilizing realistic opacities (Rajagopal & Romani 1996; Zavlin, Pavlov, & Shibanov 1996) have yielded good fits to *ROSAT* spectra of quiescent neutron stars, including quiescent spectra of 4U 2129+47 (Rutledge et al. 2000). The flux and color temperature of the spectrum are determined by the level of residual accretion and/or by the time-averaged (over 10^4–10^5 yr timescales) accretion rate in prior active phases (Brown et al. 1998). The degree to which residual heat dominates over active accretion in specific sources is a matter of current debate, with there being a recent suggestion that the quiescent flux level of 4U 2129+47 might be too low to be consistent with the cooling model (Wijnands 2002).

It is also possible that for quiescent neutron stars the "propeller effect" (Campana et al. 1998 and references therein) halts, or at least greatly diminishes, the accretion rate onto the neutron star surface. The neutron star might then enter a radio pulsar phase, with X-ray emission arising from the interaction between the pulsar wind and the accretion flow from the secondary (Campana et al. 1998; Menou et al. 1999; Campana & Stella 2000). The X-ray emission would be prominent at very large radii, comparable to the disk circularization radius. As in the outburst phase of 4U 2129+47, this would imply that the X-ray emission would be gradually eclipsed over $\gtrsim 0.1$ in orbital phase.

A number of neutron star systems in quiescence have exhibited hard tails (Asai et al. 1996, 1998; Campana et al. 1998; Rutledge et al. 2001), which might be related to the shocked pulsar wind. The shocked wind emission might be in addition to and somewhat independent of any emission associated with the neutron star surface; i.e., the hard tail could vary, while the soft excess remained steady (Campana & Stella 2000). The presence or absence of such a hard tail in the quiescent state of 4U 2129+47 has been impossible to determine with *ROSAT* observations (0.1–2.4 keV), although those observations did suggest that the soft X-ray component was variable (Garcia 1994; Garcia & Callanan 1999).

4U 2129+47 has another very interesting property that relates to estimates of its quiescent flux. After 4U 2129+47 entered quiescence, optical modulation was no longer observed over its 5.24 hr binary period. Instead of finding its expected M- or K-type companion, a nearby late F-type star was found (Kaluzny 1988; Thorstensen et al. 1988; Chevalier et al. 1989; Garcia et al. 1989; Cowley & Schmidtke 1990), which has led to the hypothesis that the 4U 2129+47 system is a hierarchical triple. The F star would be in a few month orbit about the inner binary, which in turn could lead to modulations of the binary eccentricity on 50 yr timescales (Garcia et al. 1989). It is the optical measurements of this F star, which may or may not be related to the X-ray source, that yield the 6.3 kpc distance that has been used by Garcia et al. (2001) to determine the quiescent flux of 4U 2129+47. We note that given a 6.3 kpc distance, 4U 2129+47 is the third brightest quiescent neutron star in the Garcia et al. (2001) sample.

The *Chandra* X-ray satellite, which provides excellent spatial resolution ($\lesssim 1''$) and good coverage in the soft X-ray band (0.5–10 keV), can help answer some of the questions concerning the 4U 2129+47 system. The high spatial resolution can determine whether or not the X-ray source is truly coincident with the observed F star. Measurement of the eclipse can determine whether an extended coronal structure still exists and place constraints on the mass and radius of the secondary. The 0.5–2 keV spectra can yield constraints on surface emission models, while the 2–10 keV spectra can indicate whether 4U 2129+47 exhibits a hard tail similar to other quiescent neutron stars. To these ends, on 2000 December 9, we obtained a 37 ks ($\approx$two binary orbital periods) observation of 4U 2129+47. Details of the observational modes and data extraction methods are presented in § 2.

The discussion of our results is organized as follows: We first outline our data extraction methodology in § 2. In § 3 we discuss the previous optical observations and the extent to which the X-ray source is coincident with the identified F star. We then present the X-ray light curve in § 4 and discuss its implications. We present orbital phase–resolved spectroscopy in § 5. We summarize our results in § 6 and suggest further observations with *XMM-Newton* that can resolve the mysteries left unanswered by these *Chandra* observations. So as not to deter the reader from the scientific results, some of the details of the analyses are relegated to the appendices, including discussion of the statistical methods used in analyzing the light curve (Appendix A). In Appendix B, we briefly discuss the sources that were serendipitously observed along with 4U 2129+47.

2. DATA ANALYSIS METHODOLOGY

All observations of 4U 2129+47 described here were taken with the Advanced Camera for Imaging Spectroscopy on board the *Chandra* X-ray satellite. Specifically, they were taken with the back-side–illuminated S3 chip (in imaging mode, i.e., without the gratings inserted). To reduce the amount of spectral pile-up (see below), we employed a $\frac{1}{4}$ subarray on all chips, yielding a frame readout time of 1.1 s. The total integration time was approximately 36.6 ks, with roughly a 96.5% observing efficiency (see below), yielding 35.3 ks of on-source time. Data extraction and response matrix generation were performed with the CIAO, Version 2.2, analysis package and calibration products from CALDB, Version 2.9. Sources within the field of view were detected using the WAVDETECT program, and source counts were extracted from within the 3 σ contours found from this analysis. The 4U 2129+47 background region was extracted from an annulus centered on the source with an inner radius of $5''$ and an outer radius of $14''$. We include in our spectral *and* light-curve analyses photons only in the 0.5–8 keV range and have rebinned the spectra to have between 20 and 26 photons per spectral bin. In determining the error bars of the spectral parameters, we have calculated the 90% confidence limits using the methods of Lampton, Margon, & Bowyer (1976; i.e., $\Delta\chi^2 = 2.71$ for one interesting parameter). We have not applied any systematic errors to the spectral energy bins.

Although the detected count rate from 4U 2129+47 was only $\lesssim 0.05$ counts s^{-1}, the observation did suffer from a small degree of pile-up (i.e., two photons being detected as a single photon with their summed energy). An in-depth discussion of pile-up, along with analysis methods that may be able to account partially for its effects, is presented by Davis (2001). In all fits presented in this work, we have employed

TABLE 1
Optical Identifications for the Quiescent Counterpart to the 4U 2129+47 System

Wavelength (Å)	$E(B-V)$	Distance (kpc)	Spectral Type	Reference
4500–7500.....	0.3	> 1		Thorstensen et al. 1988
4800–6600.....	0.5	4	F5–8 V	Chevalier et al. 1989
4000–4800.....			F7 IV–V	Garcia et al. 1989
3700–5600.....	0.3	6–8	F8 IV	Cowley & Schmidtke 1990
2200–3300.....	0.34		F8 IV	Deutsch et al. 1996

the pile-up model of Davis (2001) as implemented in XSPEC, ISIS, Version 1.06 (Houck & DeNicola 2000).

With a 1.1 s frame integration time and an $\approx$0.05 counts s^{-1} count rate, we expect 28 double photon events over the course of our entire observation. Roughly 95% of the detected photons land on the same 3×3 pixel region, which implies that 10% of the double photon events were registered as individual photons, whereas the remaining 90% of the double events were potentially registered as a single photon. The greatest uncertainty in the latter number is the "grade migration factor" α, i.e., the probability that the piled-up event is *not* rejected as a cosmic-ray particle or other background event. In our use of the ISIS implementation of the model of Davis (2001), we have assumed that there is a 50% probability ($\alpha = 0.5$) that two piled-up photons are accepted as a single "good event."

Consistent with the above expectations, two light-curve time bins show two distinguished photons. Since the detected spectrum peaks at $\approx$1 keV, the majority of piled-up events accepted as photons likely were read as having energy $\gtrsim$2 keV. Even though we only expect $\lesssim$26 piled-up events, as we discuss below, there are only $\approx$100 photons in the hard tail of our observed spectrum; therefore, pile-up does effect the fitted power-law slope and amplitude. If $\alpha = 0.5$ is in fact too low a probability for accepting a piled-up event, then we have undersubtracted the piled-up photons at 2 keV and slightly overestimated the value of the photon index. Likewise, if $\alpha = 0.5$ is too large, then we have slightly underestimated the photon index Γ. To date, there has been no independent calibration of the value of α (which in reality is likely to be energy- and chip location–dependent) in the *Chandra* detectors. Our estimates are that for the fits described below, these systematic effects lead to at most $\Delta\Gamma \approx \pm 0.3$.

3. ASTROMETRY

Based on the assumption of Roche lobe overflow and a main-sequence mass-radius relationship, the 5.24 hr orbital period of 4U 2129+47 suggests a secondary mass of $\approx 0.6\ M_{\odot}$, which corresponds to an M or K dwarf. It was expected that optical observations of the 4U 2129+47 system in quiescence would reveal strong ellipsoidal variations. Instead, Thorstensen et al. (1988) observed a system exhibiting an F star with no detectable orbital modulations. Comparison of the position of this quiescent optical source with the position of the optical counterpart of 4U 2129+47 in outburst revealed the two sources to be coincident within 0.″3; therefore, Thorstensen et al. (1988) considered the possibility that the 4U 2129+47 system might be a triple. With higher resolution optical observations, Chevalier et al. (1989) showed that the 4U 2129+47 field was fairly crowded but that there were no obvious contaminating sources. These authors favored the triple hypothesis. Garcia et al. (1989) found that the F star exhibited spectroscopic velocity modulations on the order of tens of kilometers per second on the timescale of months, which they also attributed to the system being a triple.

In Table 1 we list some of the optical identifications made for the quiescent counterpart to 4U 2129+47. All spectroscopic observations, ranging from 2200 to 7500 Å, agree on some type of F star identification for this counterpart, and most observations suggest an extinction of $E(B-V) \approx 0.3$. If the X-ray source is at the same distance as the F star, then it is at a distance of $\sim$4–8 kpc. (The value of 6.3 kpc used by Narayan, Garcia, & McClintock 1997b and Garcia et al. 2001 is taken from Cowley & Schmidtke 1990.) With the exquisite spatial resolution of *Chandra*, we now can also determine to what degree the X-ray source is coincident with the F star. The J2000.0 X-ray source position—R.A. = $21^{h}31^{m}26^{s}.19$, decl. = $47^{\circ}17'24''.7$—agrees very well with the coordinates of the F star observed by the *Hubble Space Telescope* (*HST*) Faint Object Spectrograph (FOS; Deutsch et al. 1996).

The spatial coincidence can be further tested with the *HST* images obtained (separately from the FOS spectra) by Deutsch et al. (1996). In addition to the image of the F star, the *HST* observations also contain a likely counterpart for the source S3-δ listed in Appendix B. The S3-δ X-ray source, likely a star, has 28 photons detected over the course of the observation and therefore is well localized. Applying an $\approx 2''$ translation,[1] linear in right ascension and declination, to center the X-ray image of 4U 2129+47 on the *HST* image of the F star, it is found that the X-ray image of the S3-δ source coincides with an optical counterpart to within 0.″1. This is near the limit for differential astrometry performed with *Chandra*. The 4U 2129+47 X-ray source and the optically identified F star discussed in the references listed in Table 1 are therefore, to good accuracy, spatially coincident. In § 5 we comment further on the extent to which the F star and the quiescent X-ray counterpart of 4U 2129+47 are at the same distance.

[1] As described by threads on the *Chandra* and *HST* Web pages (http://asc.harvard.edu and http://www.stsci.edu, respectively), if one does not cross calibrate the acquired images with an accurate astrometric database, absolute astrometry errors of 0.″5–1.″5 are expected *for each instrument*. Since we are here only interested in differential astrometry, we have not attempted to absolutely calibrate the coordinates of each image field.

4. LIGHT CURVE

One of the main goals of our observation was to determine whether or not the broad, partial dip seen in the outburst light curve of 4U 2129+47 (McClintock et al. 1982; White & Holt 1982) persisted into quiescence. Garcia (1994) did not detect any evidence of an eclipse in quiescence (see below), while Garcia & Callanan (1999) found only weak evidence for an eclipse and could not distinguish among total and partial eclipse models. The folded light curve from our observation, shown in Figure 1, removes any ambiguity and shows that the eclipse is rapid, total, and of shorter duration than in outburst. The eclipse duration is 1523^{+30}_{-50} s (see Appendix A), i.e., 0.08 in binary phase. This is 2.5 times narrower than in outburst. No photons are detected over the course of the eclipse, which implies that the 3 σ upper limit to the mean observed count rate during eclipse is $\approx$0.002 counts s^{-1}. Given the mean count rate out of eclipse, the eclipsing object exhibits an optical depth of $\tau \geq 3$ with 99.9% confidence and $\tau \geq 4$ with 95% confidence.

In addition to the eclipse, the light curve exhibits a sinusoidal modulation. Fitting the light curve outside of eclipse with a function $R(\phi) = A + B\sin[2\pi(\phi - \phi_0)]$, where R is the observed rate and ϕ is the orbital phase ($\phi \equiv 0$ is the midpoint of the eclipse), we find $A = 0.037 \pm 0.002$, $B = 0.012 \pm 0.002$, and $\phi_0 = 0.60 \pm 0.03$ (90% confidence levels). Note that this sinusoidal modulation is similar to that exhibited by X1822−371 in its bright state (Parmar et al. 2000; Heinz & Nowak 2001 and references therein), where it is believed that modulation is due to interactions of the accretion stream with the accretion disk. Thus, the sinusoidal modulation may be indicating the presence of an active accretion stream and a disk about the neutron star.

Note that Garcia (1994) in three separate, short *ROSAT* High Resolution Imager (HRI) observations found evidence of variability. Because of the fact that these observations were spread over the span of a month, one could argue whether intrinsic source variability or orbital modulation was observed. The sinusoidal modulation observed here is roughly consistent, in both phase and amplitude, with the X-ray variability described by Garcia (1994; who likely detected little, if any, of the actual eclipse). Thus, whereas the quiescent light curve of 4U 2129+47 has changed from that in outburst (Garcia 1994), it is possible that the quiescent light curve has remained remarkably steady, at least in shape and *relative* amplitude, during quiescence.

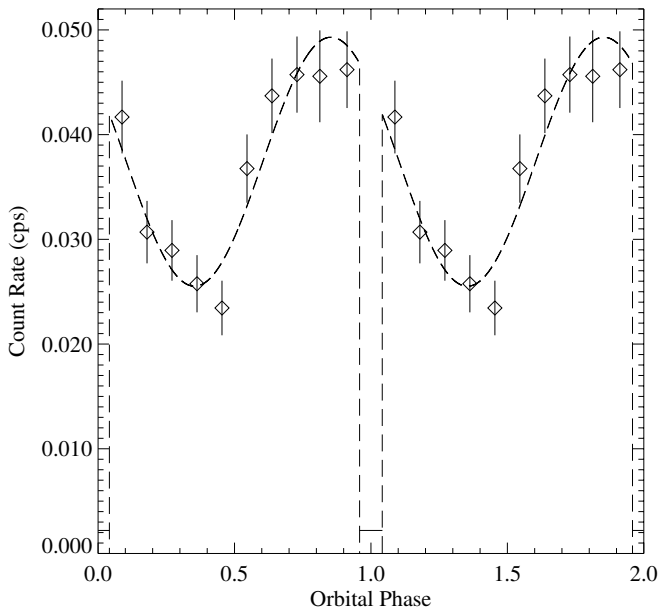

FIG. 1.—Folded 0.5–8 keV light curve of 4U 2129+47 (repeated at phases 1 and 2 for clarity). Error bars are 1 σ Poisson errors, except during the eclipse, where the horizontal bar is the 3 σ upper limit to the count rate. The dashed line shows the best-fitting sinusoidal modulation plus a total, rapid eclipse.

With an accurate measurement of the eclipse, we can update the ephemeris presented by McClintock et al. (1982). The barycenter-corrected Julian Date of the first eclipse ($\phi = 0$) in our light curve is

$$\mathrm{JD} = 2,451,879.5713 \pm 0.0002\ , \tag{1}$$

which is 0.0293 day later than expected from the McClintock et al. (1982) ephemeris. This discrepancy could be due to either the uncertainty in the original orbital period determination or orbital evolution. Adding a quadratic term to the McClintock et al. (1982) ephemeris and propagating errors, we find the time of phase zero to be

$$T_0 = 2,444,403.7429 \pm 0.002 + \left[(0.2182579 \pm 8) \times 10^{-7}\right]N \tag{2}$$

$$+ \left[(5.0 \pm 2.4) \times 10^{-11}\right]N^2\ . \tag{3}$$

(For these observations, we have observed orbits $N = 34,252$ and 34,253.) Orbital evolution is indicated, but only at the 2 σ level. Converting this into an orbital period derivative, we find

$$\dot{P}^{-1}P = (1.6 \pm 0.8) \times 10^6\ \mathrm{yr}\ . \tag{4}$$

Because of the possibility of winds, magnetic torques, etc., it can be problematic to convert an observed period derivative directly into an implied accretion rate (see, e.g., Frank, King, & Raine 1992 for a general discussion of the role of some of these effects). However, if the above period derivative is real and solely due to accretion from the secondary to the compact object, the implied accretion rate averaged over the past 20 years is $\langle \dot{M} \rangle = (4 \pm 2) \times 10^{18}$ g s^{-1}. Given that 4U 2129+47 has been in quiescence over most of this time, this would imply an extremely large accretion rate in outburst and/or substantial mass loss without radiation, i.e., an ADIOS, in quiescence. Comparably large orbital period derivatives and implied mean accretion rates have been found for X1822−371 (Parmar et al. 2000; Heinz & Nowak 2001).

We can also determine an ephemeris for the *average* period. Specifically, we have

$$T_0 = 2,451,879.5713 \pm 0.0002 + \left[(0.21825962 \pm 6) \times 10^{-8}\right]N\ , \tag{5}$$

where the period at the time of these observations might be as much as 10^{-6} days longer than the above average period.

The fact that the eclipses observed with *Chandra* are total and only 0.08 wide in phase already indicates that the X-ray emission is emanating from a region nearly 2 times smaller than in outburst. The rapidity with which eclipse ingress and egress occur, however, can place even tighter constraints. Assuming that the eclipse is total and that the

eclipsing medium has a sharp edge, then the time it takes for the count rate to go from the mean count rate down to zero, or the reverse, is indicative of the size of the X-ray source. As described in Appendix A, we have performed a statistical analysis of the eclipse ingress and egress and show the results in Figure 2. We have averaged the two ingresses with each other and the two egresses with each other, but we have not averaged the ingresses with the egresses. At the 95% confidence level, the average ingress is more rapid than 170 s, while the average egress is more rapid than 217 s. This implies that the X-ray source diameter is $\lesssim 0.07a$, where a is the binary separation. For a total system mass of 2 $M_\odot$, this implies an X-ray diameter of $\lesssim 9 \times 10^9$ cm (approximately seven Earth diameters). This is approximately a factor of 15 smaller than the implied X-ray source diameter for 4U 2129+47 in outburst (McClintock et al. 1982; White & Holt 1982).

An important caveat for the above estimates is that they pertain to the 0.5–8 keV light curve only and are dominated by emission from $\lesssim 2$ keV. Thus, we are unable to distinguish between different source sizes above and below 2 keV, as has been hypothesized (Campana et al. 1998; Campana & Stella 2000). We also note that for the most part, each individual ingress and egress looked statistically identical, with the exception of the second egress. There was weak evidence for a prolonged period of decreased emission toward the beginning of the second egress. This was most readily noted by the fact that the 1 σ limit for the second eclipse egress was 260 s, as opposed to 130–170 s for the other ingresses and egress. Accretion "dips," due to "blobs" of enhanced neutral hydrogen column, are in fact common near zero phase in Cyg X-1, for example (see Bałucińska-Church et al. 1997 and references therein). Perhaps a similar occurrence is being hinted at here, although the statistics are not strong enough to say with any degree of certainty whether or not this is the case.

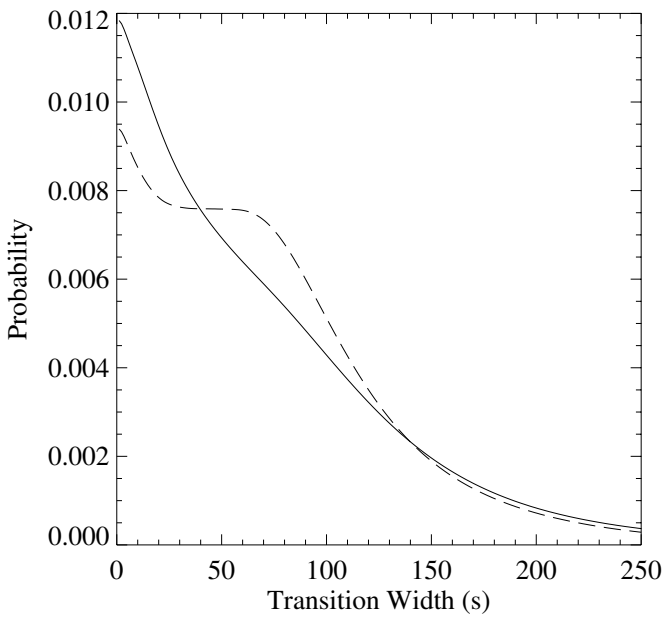

FIG. 2.—Bayesian probability distribution for the width of the eclipse ingress (*dashed line*) and egress (*solid line*), assuming a linear transition between the eclipsed and uneclipsed states.

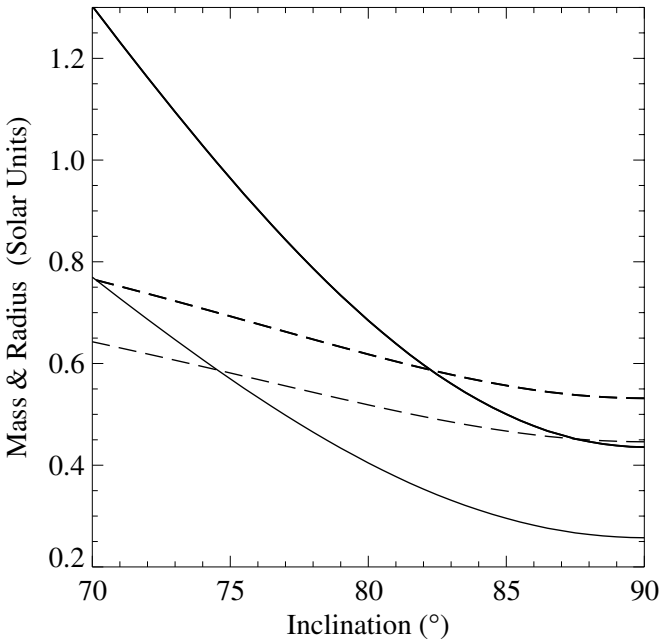

FIG. 3.—Constraints on the mass (*solid lines*) and radius (*dashed lines*) of the secondary, as a function of the system inclination. We have assumed a primary mass of 1.3 (*lower lines*) and 2.2 $M_\odot$ (*upper lines*).

The light curve not only places constraints on the X-ray source diameter, but the measured eclipse duration also places constraints on the parameters of the secondary, specifically its mass and radius.[2] Here we calculate the mass ratio of the secondary to the primary q as a function of inclination angle i. Assuming that the secondary completely fills its Roche lobe, which we approximate as spherical, then the ratio of the eclipse duration to the orbital period is given by

$$\theta \equiv \frac{\pi t_{\rm ecl}}{P_{\rm orb}} = \sqrt{\left(\frac{R_2}{a}\right)^2 - \left(\frac{\cos i}{1+q}\right)^2}\,, \tag{6}$$

where a is the orbital separation of the binary and R_2 is the Roche lobe radius of the secondary. Utilizing the approximation of Paczyński (1971), this can be rewritten as $q \approx q_0(1 - q_1)$, where

$$q_0 \equiv \tfrac{81}{8}\left(\theta^2 + \cos^2 i\right)^{3/2}, \tag{7}$$

$$q_1 \equiv \tfrac{81}{8}\left(2\cos^2 i - \theta^2\right)\left(\theta^2 + \cos^2 i\right)^{1/2}\,. \tag{8}$$

Assuming specific values for the primary mass (1.3 and 2.2 $M_\odot$), in Figure 3 we plot the secondary mass M_2 and Roche lobe radius R_2 as a function of orbital inclination.

If one takes as a straw man model that the primary is a neutron star with mass 1.3–2.2 $M_\odot$ (as evidenced by the type I burst observed by Garcia & Grindlay 1987) and that the Roche lobe radius of the secondary is greater than or equal

[2] Previous estimates of these parameters have been presented by Horne, Verbunt, & Schneider (1986) utilizing measurements taken during outburst of a sinusoidally modulated Hβ absorption line and a double-peaked He II λ4686 emission line. The two measurements together implied a primary and secondary mass of 0.6 ± 0.2 and 0.4 ± 0.2 $M_\odot$, respectively. These estimates, however, are hampered by uncertainties in modeling the outburst emission of the secondary and disk as well as by any possible contamination from the F star.

to its main-sequence radius (as has been measured for the secondary in numerous accreting systems), then the eclipse measurements alone imply that the system inclination $i > 75^\circ$ and that for the secondary mass $0.25\ M_\odot < M_2 < 0.6\ M_\odot$ (i.e., $0.2 \lesssim q \lesssim 0.5$).

The other interesting aspect to note about the observed light curve is that the position of the (out-of-eclipse) light-curve minimum occurs at a completely different phase than in outburst. In the light curve presented by McClintock et al. (1982), the (weak) noneclipse minimum occurred at phase ≈ 0.8. That is, the dip leads the eclipse by ≈ 0.2 in phase, similar to what is found for X1822−371 (Parmar et al. 2000; Heinz & Nowak 2001). In quiescence, the noneclipse minimum occurs at phase ≈ 0.4; i.e., it leads the eclipse by 0.6 in phase. In a model in which the minimum corresponds to the location where the accretion stream first interacts with the accretion disk, this shift can be explained if the disk has substantially shrunk in size.

As a rough illustration of this, consider a crude model in which the incoming matter has the specific angular momentum solely due to orbital motion at the inner Lagrange point and otherwise is only falling in the gravitational potential of the compact object (i.e., we are assuming $q \ll 1$). Assuming an elliptic orbit intersecting the disk, it is relatively straightforward to show that the radius of the accretion disk R_D relative to the binary separation is given by

$$\frac{R_D}{a} = \frac{x^3}{[(x^3 - 1)\cos\phi + 1]}\ , \tag{9}$$

where $x \equiv (a - R_2)/a$, R_2 is the Roche lobe radius of the secondary, and ϕ is the phase (in radians) by which the dip leads the eclipse. (The fact that here $\phi > \pi$ indicates that the approximations are not fully valid; however, they are sufficient to illustrate the general point.) Approximating the size of the Roche lobe as a function of mass ratio as above, one finds, for a broad range of q, that $R_D \approx 0.4a$–$0.5a$ for $\phi = 0.2$. This is consistent with independent estimates of the disk radius of X1822−371 (Heinz & Nowak 2001). Taking $\phi = 0.5$ and $q = 0.2$, one finds the substantially smaller value of $R_D \approx 0.2a$. More accurate estimates of the disk radius would rely on obtaining better estimates of the binary inclination and mass ratio q.

5. SPECTRUM

In Figure 4 we present the 0.5–8 keV spectrum of 4U 2129+47, averaged over all phases except the eclipse. Note that in this figure we have not corrected for photon pile-up, although we do account for this effect in our fits. Overall, the 0.5–2 keV spectrum is very similar to the *ROSAT* Position Sensitive Proportional Counter (PSPC) spectrum described by Garcia & Callanan (1999). The *Chandra* spectrum, however, clearly shows the presence of a hard tail, even after accounting for pile-up, that lies beyond the upper energy cutoff of *ROSAT*.

As a first description of the *Chandra* spectrum, we fit a model consisting of a blackbody plus power law that is absorbed by a neutral column (utilizing the absorption model of Wilms, Allen, & McCray 2000). Results of this fit are presented in Table 2 (model A), where we have parameterized the blackbody normalization by an effective radius R, equivalent to assuming an emitting area of πR^2 and a source distance of 6 kpc. The power-law flux is for the photon index being $\propto E^{-\Gamma}$, and the power-law normalization is in units of photons $\mathrm{keV}^{-1}\ \mathrm{cm}^{-2}\ \mathrm{s}^{-1}$ at 1 keV. (Note the large error bars on this normalization are more indicative of the uncertainties in the power-law slope, as opposed to the flux uncertainties at energies greater than 2 keV.) The neutral column, blackbody temperature, and implied flux we obtain are consistent with the fits to PSPC observations described by Garcia & Callanan (1999), which were also averaged over phase. The flux and spectrum of 4U 2129+47 are therefore consistent with having remained constant since 1994.[3]

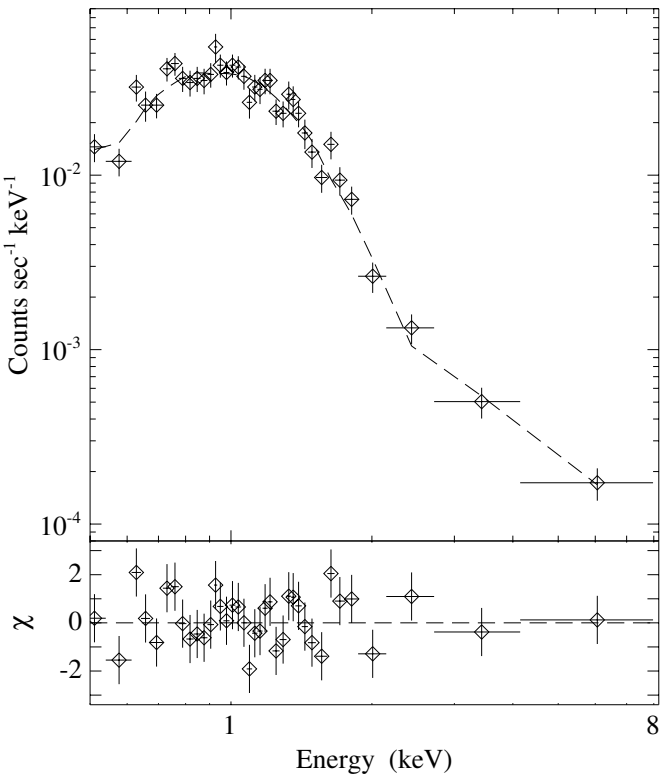

FIG. 4.—Measured 0.5–8 keV spectrum of 4U 2129+47, *excluding* the eclipses, fitted with an absorbed blackbody plus power law. The lower panel shows the residuals from this fit.

The fitted radius of less than 4 km (90% confidence levels) for these observations is significantly smaller than the ≈ 10 km expected for a neutron star; however, as discussed by Rutledge et al. (2000), this might be attributed to the fact that a simple blackbody is not the correct model for a realistic neutron star atmosphere. Numerous theoretical models exist that more carefully treat the radiative transfer in such an atmosphere. To describe the *Chandra* spectra of 4U 2129+47, we here use an XSPEC (Arnaud 1996) implementation of the model of Zavlin et al. (1996). Fitted parameters for this model include neutron star temperature, mass, radius, and distance. For all fits described here, we have fixed the neutron star mass to 1.4 $M_\odot$. As presented in Table 2, we have performed fits with a fixed distance of 6 kpc (model C) and fixed radii of 10 (model E) and 5 km

[3] Earlier *ROSAT* HRI observations (Garcia 1994) lacked any detailed spectral information. However, assuming the same model as for the PSPC fits, Garcia & Callanan (1999) argued that during the 1992 HRI observations, 4U 2129+47 was approximately a factor of 2 more luminous. Rutledge et al. (2000), using neutron star atmosphere models, also argued that 4U 2129+47 was likely more luminous during the HRI observations.

TABLE 2
FITS TO THE X-RAY SPECTRA OF 4U 2129+47 (90% CONFIDENCE LEVEL ERROR BARS)

Fit	$N_{\rm H}$ ($\times 10^{21}$ cm^{-2})	kT (keV)	R or D [a] (km or kpc)	A_Γ ($\times 10^{-6}$)	Γ	0.5–2 keV [b] ($\times 10^{-13}$ erg cm^{-2} s^{-1})	0.5–2 keV [c] ($\times 10^{-13}$ erg cm^{-2} s^{-1})	2–8 keV ($\times 10^{-13}$ erg cm^{-2} s^{-1})	χ^2 / dof
A.....	$3.1^{+0.9}_{-0.7}$	$0.21^{0.02}_{0.03}$	$2.5^{1.5}_{0.7}$	$6.4^{20.2}_{5.2}$	$1.1^{1.1}_{1.1}$	1.0	2.5	0.5	38.1 / 33
B.....	$2.0^{0.9}_{0.8}$	$0.22^{0.03}_{0.02}$	$2.1^{1.0}_{0.7}$	$2.8^{10.0}_{2.4}$	$0.6^{1.1}_{1.3}$	1.3	2.5	0.5	37.3 / 31
	$4.3^{1.1}_{1.0}$	...	...	...	...	0.8	...	...	...
C.....	$3.4^{0.3}_{0.4}$	$0.25^{0.00}_{0.06}$	$5.0^{+0.9}$ [d]	$2.1^{0.5}_{1.8}$	$0.4^{0.6}_{1.1}$	1.0	2.9	0.5	38.2 / 33
D	$2.7^{0.4}_{0.7}$	$0.24^{0.01}_{0.13}$	$5.0^{+2.4}$ [d]	$1.5^{5.2}_{1.3}$	$0.2^{1.1}_{1.4}$	1.3	3.1	0.5	38.0 / 31
	$5.0^{0.6}_{1.0}$	...	...	...	...	0.8	...	...	...
E.....	$4.2^{1.2}_{0.9}$	$0.08^{0.03}_{0.02}$	$1.9^{2.1}_{1.2}$	$4.6^{20.1}_{3.9}$	$0.9^{1.3}_{1.4}$	1.0	4.0	0.5	37.6 / 33
F.....	$3.2^{1.1}_{1.1}$	$0.10^{0.02}_{0.01}$	$2.7^{3.3}_{1.6}$	$2.2^{8.1}_{2.0}$	$0.4^{1.2}_{1.4}$	1.3	4.0	0.5	37.9 / 31
	$5.4^{1.4}_{1.2}$	...	...	...	...	0.8	...	...	...
G	$3.9^{1.0}_{0.9}$	$0.22^{0.05}_{0.05}$	$4.2^{3.6}_{2.2}$	$3.7^{15.8}_{3.3}$	$0.8^{1.2}_{1.3}$	1.0	3.6	0.5	37.4 / 33
H	$2.8^{1.1}_{0.8}$	$0.25^{0.05}_{0.05}$	$5.8^{4.2}_{3.0}$	$1.6^{8.2}_{1.5}$	$0.3^{1.2}_{1.6}$	1.3	3.6	0.5	38.0 / 31
	$5.1^{1.3}_{1.1}$	...	...	...	...	0.8	...	...	...

[a] Neutron star radius (km) assuming a distance of 6 kpc (A–D) or neutron star distance (kpc) assuming a radius of 10 (E–F) or 5 km (G–H).
[b] Absorbed flux.
[c] Unabsorbed flux.
[d] Lower limit set by table boundaries of neutron star atmosphere model.

(model G). The parameter space for these fits contains a number of local χ^2 minima, and the "best-fit" parameters and their associated error bars describe the statistics within the parameter regions of these local minima.

We see that fixing the distance at 6 kpc leads to good fits with a slightly larger neutron star radius of $\gtrsim 5$ km and a temperature very similar to that of the simple blackbody fit. Postulating a larger neutron star radius of 10 km yields a lower temperature of ≈ 0.1 keV—consistent with that found by Rutledge et al. (2000) using these same models to describe the PSPC data; however, the inferred distance is then rather small. The 90% confidence upper limit of less than 4 kpc is less than most of the distance estimates based on optical studies of the F star. (Note that the fit with the fixed 10 km radius also yielded the largest fitted value of the neutral column.) Assuming instead a neutron star radius of 5 km yields distance estimates consistent with those of the F star.

It had already been noted by Garcia & Callanan (1999) that the neutral column obtained from the orbital phase–averaged *ROSAT* PSPC spectrum was too large to be consistent with the reddening of the F star. Using our typical fitted column of 4×10^{21} cm^{-2} implies $E(B-V) \approx 0.75$ (Predehl & Schmitt 1995), whereas the $E(B-V) = 0.34$ measured by Deutsch et al. (1996) implies a column of 1.9×10^{21} cm^{-2}. Phase-resolved spectroscopy offers a possible solution to this discrepancy. As shown in Figure 1, there is clear phase-dependent variability. Extracting spectra at orbital phases 0.2–0.5 and 0.65–0.958, the variation appears to be consistent with changes in the soft spectrum only. (The statistics of the hard tail above 2 keV become poor in each phase bin but are consistent with a constant amplitude and slope.) We therefore have chosen to perform a series of fits where below 2 keV we consider the above two orbital phases, while above 2 keV we use the spectrum from the total observation, excluding the eclipse. We constrain all model parameters, including normalizations, to be the same for each of these spectra, except that we allow the neutral column to be different in each orbital phase. (For the hard tail, we constrain the neutral column to be the same as for orbital phases 0.65–0.958.) All three spectra are fitted simultaneously, and the results are presented in Table 2 and Figure 5. As for our orbital phase–averaged spectra, we present a simple blackbody model (model B) and neutron star atmosphere models with fixed distances (model D) or radii (models F and H).

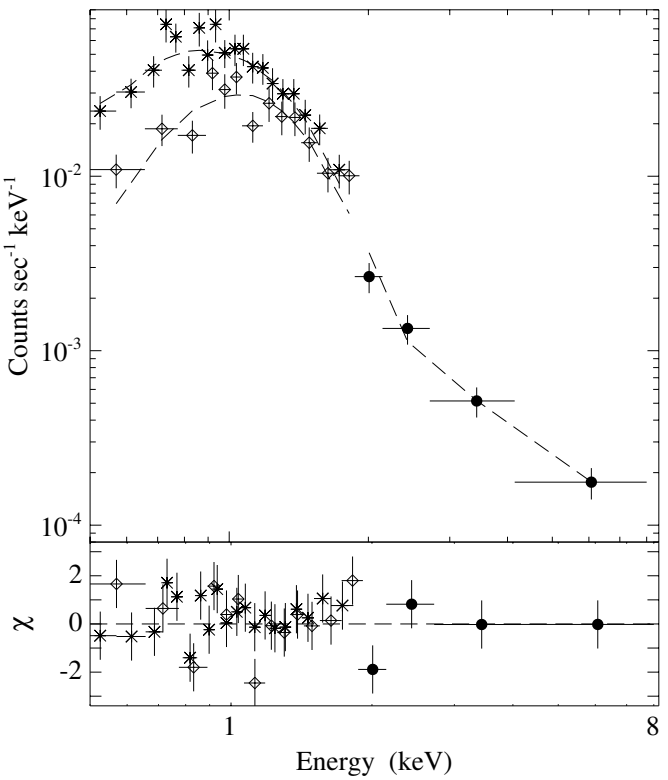

FIG. 5.—Phase-resolved spectra of 4U 2129+47 (*upper panel*). The filled circles represent the 2–8 keV spectrum, measured from all phases excluding the eclipses. The diamonds and asterisks represent the spectrum integrated over phases 0.65–0.96 and 0.2–0.5, respectively. The dashed line is the best-fit absorbed blackbody plus power-law model where all parameters, except neutral hydrogen column, were constrained to be identical as a function of phase. The lower panel shows the contribution to the χ^2 of the residuals from this fit.

Overall these fits are fairly good, and we see that the fitted temperatures, radii, distances, and power-law parameters are very comparable to those obtained for the phase-averaged fits. The neutral column is seen to vary by nearly a factor of 2 between the two phases, with the lower column value being a factor of only 10%–70% larger than would be implied by the F star reddening. The averages of the two column values are approximately the same as the columns determined from the phase-averaged fits. The spectral variations are therefore consistent with being solely due to variations of the intrinsic column, with the total column having roughly equal contributions from intrinsic and extrinsic columns.

As regards the power-law components in these fits, all fits imply that the power law comprises $\gtrsim 10\%$ of the (unabsorbed) 0.5–8 keV flux. The error bars are large; however, the index of the power law is consistent with being fairly flat. We note that, if anything, changing our assumptions regarding pile-up is most likely to further flatten the power law (see § 2). In terms of amplitude, slope, and extent, such a power law is difficult to describe solely using a neutron star atmosphere model.

6. DISCUSSION

Our *Chandra* observations of 4U 2129+47 have revealed that the previously observed extended coronal structure has collapsed by at least a factor of 15 in size. The soft X-ray spectrum is now consistent with thermal emission from the surface of a neutron star with a radius on the order of 5 km. To what extent this emission is indicative of residual thermal emission or active, albeit low-level, accretion remains unclear. The fact that the spectrum observed by *Chandra* is consistent in amplitude and shape with that observed by *ROSAT* in 1994 can easily be accommodated for in the cooling neutron star model since the cooling timescale is expected to be very long. The prior observed soft X-ray variability (Garcia 1994) can be accounted for via orbital phase–dependent obscuration effects rather than intrinsic accretion variability.

On the other hand, questions concerning the cooling model remain. First, assuming a distance of 6 kpc, consistent with various estimates of the F star distance, the fitted neutron star radius tends to be fairly low, on the order of 5 km. Although larger than the inferred blackbody radius, this is smaller than expectations from numerous neutron star models. Forcing a large neutron star radius, 10 km, implies a distance substantially less than most estimates of the F star distance, which of course might still be a chance overlap. However, it is seen that each of the various fits, including the simple blackbody, are statistically nearly identical to one another. Second, the variability discussed by Garcia (1994) is consistent, in amplitude and phase, with that observed here, which indicates that roughly $\frac{2}{3}$ of the integration time from the 1992 HRI observation occurred over the phases of *lowest* emission. Thus, the estimate of an approximate factor of 2 flux difference between 1992 and 1994 might be an *underestimate*, although this is hampered by the poor spectral resolution of the HRI. Rutledge et al. (2000) argue that this change might be related to solely the outer crust cooling. Additionally, this change in flux might indicate that as of 1992, 4U 2129+47 had not yet truly entered into a quiescent phase.

Based on the work of Brown et al. (1998) and the observations discussed by Garcia (1994), Garcia & Callanan (1999), and Rutledge et al. (2000), Wijnands (2002) has suggested that the quiescent phase of 4U 2129+47 might be too faint to be consistent with the neutron star cooling model. Specifically, one expects a quiescent flux of

$$F_q \approx \frac{t_o}{t_o + t_q} \frac{\langle F_o \rangle}{135} , \tag{10}$$

where $\langle F_o \rangle$ is the average flux in outburst, t_o is the average time the source spends in outburst, and t_q is the average time spent in quiescence. Assuming a typical accretion efficiency of $\epsilon \sim 0.1$ and an average accretion rate of $\langle \dot{M} \rangle \sim 4 \times 10^{18}$ g s^{-1}, as suggested by the possible period derivative found in § 4, we then find that

$$\frac{t_q}{t_o} \gtrsim 10^3 \left(\frac{D}{6 \text{ kpc}} \right)^2 \left(\frac{\epsilon}{0.1} \right) . \tag{11}$$

To accommodate the above result, either the assumed accretion rate is atypically large (i.e., not indicative of the long-term average in outburst), the durations of the quiescent periods are very long, there is enhanced cooling of the neutron star during quiescence (see Wijnands 2002; Wijnands, Heinke, & Grindlay 2002 and references therein), or the efficiency is very low.

If one instead assumes an average outburst flux of $\langle F_q \rangle \sim 2 \times 10^{-9}$ ergs cm^{-2} s^{-1} (i.e., 5 times the typical 2–10 keV flux seen in outburst; Garcia & Grindlay 1987 and references therein), then one obtains $t_q/t_o \gtrsim 20$. However, this estimate assumes that one has observed nearly all of the outburst flux in the system, contrary to the more usual assumptions for an ADC of either a very optically thin or very optically thick corona seen near edge-on (Parmar et al. 2000; Heinz & Nowak 2001). In order to retain the typical ADC assumptions, one is again drawn toward hypotheses of the previous outburst episode being atypically bright, long quiescent periods, enhanced neutron star cooling, or very low radiative efficiencies. Given that any matter that reaches the neutron star surface will contribute toward heating the neutron star, the latter hypothesis implies that inefficiency during outburst is achieved via an outflow, e.g., an ADIOS.

Questions remain about the origin of the sinusoidal variability and the power-law tail. The former is similar to what has been observed in X1822−371, where the variability has been associated with the interaction of the accretion stream with the outer edge of an accretion disk (Parmar et al. 2000; Heinz & Nowak 2001). A similar model for 4U 2129+47 could argue for active accretion. Observations of X1822−371 imply that a totally opaque disk rim is raised that completely blocks the central neutron star, while a more vertically extended disk atmosphere (with $N_{\rm H} \lesssim 10^{22}$ cm^{-2}) attenuates the extended corona (Heinz & Nowak 2001). Here the evidence suggests that the neutron star in 4U 2129+47 is directly observable, while the combination of inclination angle and outer disk atmosphere height serves only to attenuate its soft flux with a column of $N_{\rm H} \approx 2 \times 10^{21}$ cm^{-2}. The presence of the hard tail might also argue for active accretion. The limited *Chandra* bandpass shows that at least $\gtrsim 10\%$ of the total, unabsorbed 0.5–8 keV luminosity emanates from this component. Thus, we might be seeing the accretion energy first being funneled

through a corona and then actively being dissipated as thermal energy on the neutron star surface.

One alternative that preserves the cooling model would be for the accretion stream to be halted by an outgoing pulsar wind (Campana et al. 1998; Menou et al. 1999; Campana & Stella 2000). The hard tail would represent shocked emission from the interaction region of the wind and accretion stream. The sinusoidal modulation could still be due to a neutral hydrogen column being raised by the interaction of the accretion stream with a disk rim. Such a disk need not be actively accreting, however, since the pulsar wind and magnetic field could halt any inward flow of disk material. We note that the disk radius inferred from the location of the light-curve minimum is comparable to expectations from the pulsar wind model; however, the soft flux radius determined from the rapidity of the eclipse is somewhat smaller.

The *Chandra* observations have lent further credence to the hypothesis that the 4U 2129+47 system is a hierarchical triple. The X-ray source position is now seen to be even more closely aligned with optical position of the F star. Furthermore, the minimum fitted neutral column (i.e., the flux from the maximum emission phase of the light curve) is more consistent with the reddening of the F star than were previous measurements obtained from phase-averaged spectra.

Prospects are good for refining the answers to some of the remaining questions about 4U 2129+47. Further observations with either *Chandra* or *XMM-Newton*, aside from improving the statistics of the model fits, might reveal variability. Variability in the soft spectra would argue against the cooling model being the sole source of quiescent emission. *XMM-Newton* observations can have direct bearing on the pulsar wind models for the hard tail. Aside from extending detection of this tail to beyond 8 keV (which would rule out most atmosphere models for the hard tail), the methods of § 4 then could be applied separately to the hard tail. Measurement of three or more eclipses would allow one to place limits of $\approx 0.1a$ on the diameter of the hard component emission region. Although large, this is a smaller diameter than suggested by many of the pulsar wind models.

Additionally, each *XMM-Newton* observation can determine the eclipse centroid to approximately ± 8 s. If the F star is truly in a month-long orbit about the binary, then we expect ± 80 s variations in the eclipse ephemeris. Thus, multiple *XMM-Newton* observations spaced out over a month-long timescale could directly determine the orbital parameters of a third body. In the absence of the detection of such orbital variations, either *Chandra* or *XMM-Newton* observations could determine whether or not the orbital period evolution hinted at in the analysis of § 4 actually occurred. This in turn, as discussed above, could have implications for the expected level of quiescent emission in the cooling neutron star model.

We would like to acknowledge C. Bailyn, L. Bildsten, J. Davis, J. McClintock, and T. Maccarone for useful conversations and P. Maloney for providing a moment of Zen. M. A. N. would like to acknowledge the hospitality of the Yale Astronomy Department, where much of this work was carried out. We thank V. Zavlin for providing us with the XSPEC implementation of the neutron star atmosphere code. Support for this work was provided by the National Aeronautics and Space Administration through *Chandra* Award G00-2038X issued by the *Chandra* X-ray Observatory Center, which is operated by the Smithsonian Astrophysical Observatory for and on behalf of NASA under contract NAS 8-39073.

APPENDIX A

ECLIPSE ANALYSIS

In what follows, we explicitly ignore the effects of detector "dead time." Each *Chandra* frame for this observation represented an integration time of approximately 1.1 s with a "frame transfer time" of 40 ms between frames.[4] The effective deadtime therefore was on the order of 3.5%, which is negligible for the purposes of this analysis. We shall employ a Bayesian approach.

The following discussion pertains to eclipse egress; however, it is readily generalized to ingress as well. We label our $\Delta t = 1.1$ s time bins with indices $0 \rightarrow k$ and assume that at the beginning of the time bin indexed by 0, the X-ray source is fully eclipsed and by the beginning of the time bin indexed by k it is fully unobscured. We assume that the mean count rate measured at the detector increases linearly from 0 to r (although other assumptions are readily accommodated). The mean count rate in time bin i is therefore $r_i = r(i + \frac{1}{2})/k$, for $i = 0 \rightarrow k - 1$. Following the usual derivation of Poisson statistics, we assume that each bin is short enough such that the probability of measuring one photon event in a given bin is $P(1) = r_i \Delta t$, the probability of measuring no events is $P(0) = 1 - P(1)$, and that $P(> 1) = 0$. The probability of the data D given this model is therefore

$$P(D|r, k) = \prod_i r_i \Delta t \prod_j (1 - r_j \Delta t) \ , \tag{A1}$$

where the product over i is for those bins where a photon was detected and the product over j is for those bins where no photons were detected. We divide the above by the probability assuming a steady, uneclipsed count rate of r, which, given $r \ll 1$, yields

$$P(D|r, k) \propto \prod_i \left(\frac{r_i}{r}\right) \prod_j [1 + (r - r_j)\Delta t] = \prod_i \left(\frac{i + 1/2}{k}\right) \prod_j \left[1 + r\Delta t \left(\frac{k - j - 1/2}{k}\right)\right] \ . \tag{A2}$$

[4] See the *Chandra* Proposer's Observatory Guide at http://cxc/harvard.edu.

Further approximating the product over empty time bins as the exponential of a sum, taking a uniform prior for k (the eclipse sharpness) and a Gaussian prior for the detected count rate, and employing Bayes theorem, we obtain the probability distribution for the model parameters as

$$P(r, k|D) \propto \exp\left[\frac{-(r-\bar{r})^2}{2\sigma_r^2}\right] \prod_i \left(\frac{i+1/2}{k}\right) \exp\left[r\Delta t \sum_j \left(\frac{k-j-1/2}{k}\right)\right] . \quad \text{(A3)}$$

In practice, based on the fits to the folded light curve, we have used $\bar{r} = 0.046$ and 0.042 counts s^{-1} for the mean ingress and egress count rates, respectively, and we have taken $\sigma_r = 0.0035$ counts s^{-1} for both. In the above we have assumed a fixed start point for the egress commencement. We allow for uncertainty in this start point by assuming that its prior probability is uniformly distributed between 0 and 500 s before the first detected photon. Equation (A3) then must be slightly modified by including in the sum within the exponential all the time bins from 500 s before the first detected photon to the time bin represented by index 0.

The above was used to calculate probability distributions separately for the two measured eclipse ingresses and the two measured eclipse egresses. The probability distributions were then multiplied together for each pair to give the ingress and egress distributions for the folded light curve. Marginalizing over the eclipse sharpness yielded the eclipse widths and midpoints, while marginalizing over the eclipse start points yielded the distributions for the eclipse sharpness (see § 4).

APPENDIX B

SERENDIPITOUSLY OBSERVED SOURCES

A number of other sources were serendipitously observed within a few arcminute radius of 4U 2129+47. These sources, along with their coordinates and 0.3–8 keV total counts (i.e., integrated over the entire 36.6 ks observation), are presented in Table 3. For the most part, these sources can be identified with stellar objects in the Digital Sky Survey.[5] Several sources, specifically S3-β, S2-α, I2-α, and I3-α, might be faint active galactic nuclei. S3-β contains sufficient counts to fit a crude spectrum, and it is found to be consistent with an absorbed power law, with $N_{\rm H} = (3 \pm 3) \times 10^{21}$ cm^{-2} and $\Gamma = 1.9 \pm 0.6$, with 90% confidence limits. Its 0.5–8 keV (absorbed) flux corresponds to 4×10^{-14} ergs cm^{-2} s^{-1}. There is also weak evidence that its count rate increases by a factor of 2 on timescales of $\approx$25 ks.

The source S3-δ was useful for performing differential astrometry since it likely was detected also with the *HST* observations of Deutsch et al. (1996). For purposes of differential astrometry (as opposed to Table 3), the source position was determined with the program WAVDETECT applied to the 0.5–2 keV image.

Note that given the broad energy range (0.3–8 keV) and large confidence contours (3 σ detection region from WAVDETECT), the total counts in Table 3 might contain photons unrelated to the source and therefore should be regarded as upper limits. This is especially true as the angular distance from the target point, S3-α, increases.

[5] See http://www-gsss.stsci.edu/DSS/dss_home.htm.

TABLE 3
SOURCES IN THE *Chandra* FIELD

Source[a]	R.A. (J2000.0)	Decl. (J2000.0)	Counts (0.3–8 keV)[b]
S3-α	21 31 26.19	47 17 24.7	1301
S3-β	21 31 24.57	47 17 12.7	205
S3-γ	21 31 30.29	47 16 16.5	36
S3-δ.....	21 31 27.86	47 17 32.5	28
S3-ϵ.....	21 31 29.21	47 16 36.9	25
S2-α	21 31 34.64	47 15 3.6	88
S2-β	21 31 33.18	47 15 4.3	9
I2-α.....	21 30 55.13	47 09 49.6	115
I3-α.....	21 30 27.83	47 15 23.5	80

NOTE.—Units of right ascension are hours, minutes, and seconds, and units of declination are degrees, arcminutes, and arcseconds.

[a] Chip ID source identifier (brightest to faintest).

[b] Counts from within the 3 σ detection region as determined via WAVDETECT.

REFERENCES

Arnaud, K. A. 1996, in ASP Conf. Ser. 101, Astronomical Data Analysis Software and Systems V, ed. J. H. Jacoby & J. Barnes (San Francisco: ASP), 17
Asai, K., Dotani, T., Hoshi, R., Tanaka, Y., Robinson, C. R., & Terada, K. 1998, PASJ, 50, 611
Asai, K., Dotani, T., Mitsuda, K., Hoshi, R., Vaughan, B., Tanaka, Y., & Inoue, H. 1996, PASJ, 48, 257
Bałucińska-Church, M., Takahashi, T., Ueda, Y., Church, M. J., Dotani, T., Mitsuda, K., & Inoue, H. 1997, ApJ, 480, L115
Bildsten, L., & Rutledge, R. E. 2001, in The Neutron Star–Black Hole Connection, ed. C. Kouveliotou, J. Ventura, & E. P. J. van den Heuvel (NATO ASI Ser. C, 567; Dordrecht: Kluwer)
Blandford, R. D., & Begelman, M. C. 1999, MNRAS, 303, L1
Brown, E. F., Bildsten, L., & Rutledge, R. E. 1998, ApJ, 504, L95
Campana, S., & Stella, L. 2000, ApJ, 541, 849
Campana, S., Stella, L., Mereghetti, S., Colpi, M., Tavani, M., Ricci, D., Fiume, D. D., & Belloni, T. 1998, ApJ, 499, L65
Chevalier, C., Ilovaisky, S. A., Motch, C., Pakuli, M., & Mouchet, M. 1989, A&A, 217, 108
Cowley, A. P., & Schmidtke, P. C. 1990, AJ, 99, 678
Davis, J. E. 2001, ApJ, 562, 575
Deutsch, E. W., Margon, B., Wachter, S., & Anderson, S. F. 1996, ApJ, 471, 979
Esin, A. A., McClintock, J. E., & Narayan, R. 1997, ApJ, 489, 865
Frank, J., King, A., & Raine, D. 1992, Accretion Power in Astrophysics (2d ed.; Cambridge: Cambridge Univ. Press)
Garcia, M. R. 1994, ApJ, 435, 407
Garcia, M. R., Bailyn, C. D., Grindlay, J. E., & Molnar, L. A. 1989, ApJ, 341, L75
Garcia, M. R., & Callanan, P. J. 1999, AJ, 118, 1390
Garcia, M. R., & Grindlay, J. E. 1987, ApJ, 313, L59
Garcia, M. R., McClintock, J. E., Narayan, R., Callanan, P. J., & Murray, S. S. 2001, ApJ, submitted
Heinz, S., & Nowak, M. A. 2001, MNRAS, 320, 249
Horne, K., Verbunt, F., & Schneider, D. P. 1986, MNRAS, 218, 63
Houck, J. C., & DeNicola, L. A. 2000, in ASP Conf. Ser. 216, Astronomical Data Analysis Software and Sytems IX, ed. N. Manset, C. Veillet, & D. Crabtree (San Francisco: ASP), 591
Kaluzny, J. 1988, Acta Astron., 38, 207
Lampton, M., Margon, B., & Bowyer, S. 1976, ApJ, 208, 177
McClintock, J. E., London, R. A., Bond, H. E., & Grauer, A. 1982, ApJ, 258, 245
Menou, K., Esin, A. A., Narayan, R., Garcia, M. R., Lasota, J.-P., & McClintock, J. 1999, ApJ, 520, 276
Narayan, R., Barret, D., & McClintock, J. E. 1997a, ApJ, 482, 448
Narayan, R., Garcia, M. R., & McClintock, J. E. 1997b, ApJ, 478, L79
Paczyński, B. 1971, ARA&A, 9, 183
Parmar, A. N., Oosterbroek, T., Del Sordo, S., Segreto, A., Santangelo, A., Fiume, D. D., & Orlandini, M. 2000, A&A, 356, 175
Predehl, P., & Schmitt, J. H. M. M. 1995, A&A, 293, 889
Rajagopal, M., & Romani, R. W. 1996, ApJ, 461, 327
Rutledge, R. E., Bildsten, L., Brown, E. F., Pavlov, G. G., & Zavlin, V. E. 2000, ApJ, 529, 985
———. 2001, ApJ, 551, 921
Thorstensen, J. R., et al. 1988, ApJ, 334, 430
van Paradijs, J., Verbunt, F., Shafer, R. A., & Arnaud, K. A. 1987, A&A, 182, 47
White, N. E., & Holt, S. S. 1982, ApJ, 257, 318
Wijnands, R. 2002, in ASP Conf. Ser., X-Rays at Sharp Focus: *Chandra* Science Symposium, ed. L. K. S. Vrtilek & E. M. Schlegel (San Francisco: ASP), in press
Wijnands, R., Heinke, C. O., & Grindlay, J. E. 2002, ApJ, 572, 1002
Wilms, J., Allen, A., & McCray, R. 2000, ApJ, 542, 914
Zavlin, V. E., Pavlov, G. G., & Shibanov, Y. A. 1996, A&A, 315, 141